JOURNAL OF SOLID STATE CHEMISTRY **129,** 223–230 (1997)
ARTICLE NO. SC967221

Chemical Reactions and Dielectric Properties of the $BaTiO_3$–$LaAlO_3$ and $BaTiO_3$–$LaAlO_3$–$LaTi_{3/4}O_3$ Systems

S. Škapin, D. Kolar, and D. Suvorov

Jožef Stefan Institute, University of Ljubljana, Jamova 39, 1001 Ljubljana, Slovenia

Received October 16, 1995; in revised form October 15, 1996; accepted November 12, 1996

$BaTiO_3$–$LaAlO_3$ interaction at high temperatures results in formation of (Ba, La)(Ti, Al)O_3 solid solution, $BaAl_2O_4$, and Ba_2TiO_4. The composition of solid solution can be expressed as $Ba_{1-n}La_nTi_{1-0.52n}Al_{0.36n}O_3$ with $0 \le n \le 0.27$. Formation of secondary phases $BaAl_2O_4$ and Ba_2TiO_4 which form due to unequal solubility of La^{3+} and Al^{3+} ions into the perovskite $BaTiO_3$ lattice can be prevented by the addition of La_2O_3 and TiO_2 in ratio 2:3, i.e., as $LaTi_{3/4}O_4$. Incorporation of La and Al into $BaTiO_3$ strongly decreases the Curie temperature of $BaTiO_3$, $\approx$35 K/mol % $LaAlO_3$ added. (Ba, La)(Ti, Al)O_3 solid solution ceramics exhibit relatively low permittivities at room temperature (734–129) and very low dielectric losses, tan $\delta < 5 \times 10^{-4}$, measured at 1 MHz. The temperature stability of permittivity increases with $LaTi_{3/4}O_3$ as well with $LaAlO_3$ concentration.

1. INTRODUCTION

$BaTiO_3$-based rare earth containing ceramics exhibit valuable dielectric properties and are frequently used in manufacturing temperature stable ceramic capacitors and, more recently, for ceramic electronic components operating at microwave frequencies (1).

Rare earth ions, such as La^{3+}, can be incorporated into the $BaTiO_3$ lattice only to a limited extent. La enters the *A* sites of the $BaTiO_3$ perovskite lattice and serves as a donor. The excess charge of La^{3+} ions on Ba^{2+} sites requires electrical compensation. This may be achieved by incorporation of ions of lower valency at Ba^{2+} or Ti^{4+} sites, or by formation of effectively negatively charged defects, e.g., cation vacancies V''_{Ba}, V''''_{Ti}, anion interstitials O''_i or electrons (e'). At higher dopant levels, the La-containing $BaTiO_3$ ceramic is insulating and charge compensation is accomplished by vacancies at Ba or Ti sites. Whereas early investigators favored Ba vacancies (2–4), it was proposed later that charge compensation takes place by the creation of titanium vacancies (5). Charge compensation by titanium vacancies are further supported in (6–10).

Titanium vacancy mechanism implies the (Ba, La)TiO_3 solid solution extends on the tie line which points from $BaTiO_3$ to $LaTi_{3/4}O_3$ and may be expressed by the formula $Ba_{1-x}La_xTi_{1-x/4}(V''''_{Ti})_{x/4}O_3$ (5). The limiting solid solubility was recently determined to be $x = 0.3$ at 1400°C (10). $La_4Ti_3O_{12}$ is a 12-layer hexagonal perovskite with 3/4 of the *B* positions occupied by Ti^{4+}, i.e., $LaTi_{3/4}O_3$, which was reported to be stable up to 1450°C (11). Two other compounds along the $BaTiO_3$–$LaTi_{3/4}O_3$ tie line have been described as being stable at 1400°C; hexagonal (10 layer) $BaLa_4Ti_4O_{15}$ (5, 12, 13) and hexagonal (18 layer) $Ba_2La_4Ti_5O_{18}$ (13). Formation of defects in perovskite structure which compensate replacement of Ba^{2+} ions with La^{3+} ions may be avoided or at least diminished by simultaneous incorporation of lower valence ions on Ti^{4+} sites. It was recently shown that $La_{2/3}TiO_3$ may be effectively stabilized by forming a solid solution with $LaAlO_3$ (14). Al^{3+} ions are expected to enter the Ti sites in the $BaTiO_3$ lattice and act as acceptors (15). As such they compensate La^{3+} ions at Ba sites at room temperature.

$LaAlO_3$ crystallizes in a perovskite-like rhombohedral, nearly hexagonal structure which transforms into a simple cubic cell at 435°C (16). The compound melts congruently at $\approx$1995°C (17).

Ismailzade (18) reported solid solubility of $LaAlO_3$ in $BaTiO_3$ of up to 25 mol %. This author also observed that $LaAlO_3$ strongly decreases the Curie temperature (T_C) of $BaTiO_3$. 5 mol% $LaAlO_3$ shifted T_C to -14°C.

It was expected that the extremely low dielectric losses of $LaAlO_3$ (tan $\delta < 10^{-5}$ at 10^9 Hz) may improve the electric properties of (Ba, La)(Ti, Al)O_3 solid solutions. The aim of the present work was to investigate the structural and dielectric properties of ceramics based on $BaTiO_3$–$LaAlO_3$ solid solution ((Ba, La)(Ti, Al)O_3ss) in more detail.

2. EXPERIMENTAL PROCEDURE

Ceramic samples were prepared by the conventional powder sintering technique. The starting materials were reagent grade La_2O_3, TiO_2, Al_2O_3, and $BaTiO_3$. Materials

0022-4596/97 $25.00

were weighed, milled, dried, pressed into pellets, and calcined at 1400°C for up to 40 h with intermittent cooling, crushing, and repressing to assure equilibrium. Quenched powdered samples were examined by X-ray powder diffractometry (XRD) (Model PW 1710, Netherlands Philips, Bedrijven b. v. S&I, The Netherlands). Polished surfaces of pellets were examined by a scanning electron microscopy (SEM) (Jeol JXA 840A, Tokyo, Japan) equipped with electron probe wavelength (WDS) and energy-dispersive X-ray (EDS) analyzers using TRACOR (Model TRACOR, Series II X-ray Microanalyzer, TRACOR, The Netherlands) software for analysis.

Quantitative WDS analysis was performed by pentaerythritol (PET) (for La$L\alpha_1$, Ba$L\alpha_1$ and Ti$K\alpha_1$ lines) and by Thallium acid phthalate (TAP) (for the Al$K\alpha_1$ line) monochromators, under the following experimental conditions: 20 keV accelerating voltage and 10 nA beam current. A maximum of 0.7% standard counting deviation was allowed during the X-ray intensity measurements. $La_2Ti_2O_7$, $BaTiO_3$, and Al_2O_3 were used as standards for quantization. The PROZA (Phi-RhO-Z and A) matrix correction program (19) was applied to transform measured elemental k ratios into element concentrations. Oxygen content was calculated by difference from 100%.

To achieve acceptable density for electrical measurements, $BaTiO_3$–$LaAlO_3$ pellets had to be sintered above 1500°C, whereas excess TiO_2 decreased the sintering temperature to <1400°C. The capacitance and dielectric losses were measured at 1 MHz with a Hewlett Packard 4192A LF impedance analyzer.

TABLE 1
Phases Identified in $(1-x)BaTiO_{3-x}LaAlO_3$ Compositions after Firing at 1400°C

x (mol % $LaAlO_3$)	Phases identified[a]
1	BLTAss(t)
2	BLTAss(t)
4	BLTAss(c), BAtraces
15	BLTAss(c), BAtraces, B_2T traces
50	BLTAss(c), BA, LBATss(c), B_2T traces
90	LBATss(c), BAtraces, BLTAss(c) traces
96	LBATss(c)

[a] BLTAss(t), tetrag. (Ba, La)(Ti, Al)O_3 solid solution; BLTAss(c), cub. (Ba, La)(Ti, Al)O_3; BA, $BaAl_2O_4$, B_2T, Ba_2TiO_4; LBATss(c), cub. (La, Ba)(Al, Ti)O_3 solid solution.

3. RESULTS AND DISCUSSION

3.1. Structural and Compositional Studies

Heat treatment of $BaTiO_3$–$LaAlO_3$ mixtures results in the formation of limited solid solubility. According to the XRD results, in ceramics quenched from 1400°C it extends up to about 15 mol% $LaAlO_3$ in $BaTiO_3$. Up to 4 mol % $BaTiO_3$ remains tetragonal. With a higher amount of $LaAlO_3$ incorporated, $BaTiO_3$ solid solution (Ba, La)(Ti, Al)O_3ss is cubic. Above 15 mol% $LaAlO_3$, $BaTiO_3$-rich solid solution coexists with $LaAlO_3$-based solid solution ((La, Ba)(Al, Ti)O_3ss). $LaAlO_3$-based solid solution remains as a rhombohedral structure at up to 3 mol% $BaTiO_3$ addition, and then transforms at higher concentrations of $BaTiO_3$ into the cubic form. According to XRD data, the solid solution limit is estimated to be at 5 mol% $BaTiO_3$ in $LaAlO_3$.

The $BaTiO_3$–$LaAlO_3$ system is not binary. After heat treatment at 1400°C, besides $BaTiO_3$ and $LaAlO_3$-based solid solutions, the reaction product also contains $BaAl_2O_4$. The amount of $BaAl_2O_4$ depends on the $BaTiO_3/LaAlO_3$ ratio in the starting compositions. The maximum amount of $BaAl_2O_4$ was detected in the composition range 65–75 mol% $BaTiO_3$ and 35–25 mol% $LaAlO_3$. The maximum amount of $BaAl_2O_4$ was estimated from a comparison of X-ray peak intensities to be about 10 wt%. Besides $BaAl_2O_4$, in some samples faint XRD lines indicated the presence of Ba_2TiO_4. The results of phase analysis are shown in Table 1.

Quantitative WDS analysis of $BaTiO_3$–$LaAlO_3$ ceramics, equilibrated at 1400°C, revealed that La^{3+} and Al^{3+} ions are not incorporated in the (Ba, La)(Ti, Al)O_3ss in an

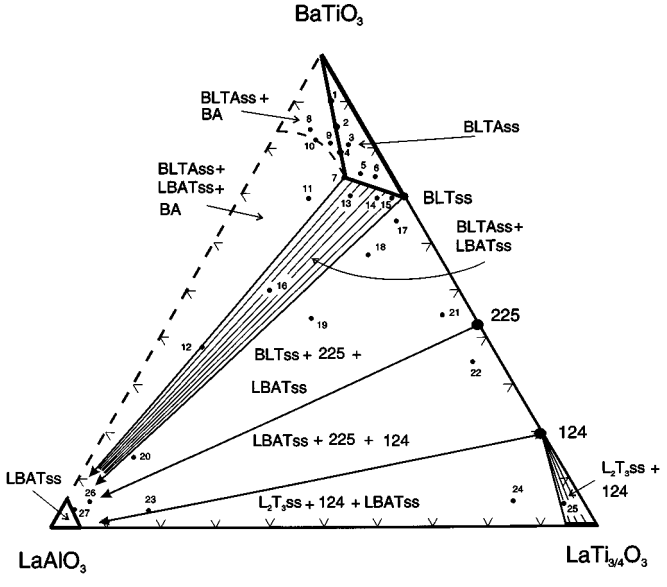

FIG. 1. Tentative subsolidus composition phase equilibrium diagram of the $BaTiO_3$–$LaAlO_3$–$LaTi_{3/4}O_3$ system at 1400°C. BLTAss, (Ba, La)(Ti, Al)O_3 solid solution; BLTss, (Ba, La)TiO_3 solid solution; LBATss, (La, Ba)(Al, Ti)O_3 solid solution; 225, $Ba_2La_4Ti_5O_{18}$; 124, $BaLa_4Ti_4O_{15}$; L_2T_3ss, $LaTi_{3/4}O_3$ solid solution (containing some La and Al); BA, $BaAl_2O_4$.

TABLE 2
Results of the WDS Microanalysis of the (Ba, La)(Ti, Al)O_3 Phase in $(1-x)BaTiO_3$–$xLaAlO_3$ Samples after Firing at 1400°C and Their Calculated Formulas

Composition x in $(1-x)$ $BaTiO_3$: x $LaAlO_3$	Measured (at.%):				Normalized to Ba + La + Ti + Al + V_{Ti} + $O_{stoic.}$ = 100%					Calculated formula
	Ba	La	Ti	Al	Ba	La	Ti	Al	V_{Ti}	
0.06	18.51	1.42	19.26	0.52	18.53	1.42	19.28	0.52	0.23	$Ba_{0.93}La_{0.07}Ti_{0.96}Al_{0.03}V_{(Ti)0.01}O_3$
0.10	16.70	1.84	17.32	0.68	18.16	2.00	18.84	0.74	0.32	$Ba_{0.90}La_{0.10}Ti_{0.94}Al_{0.04}V_{(Ti)0.02}O_3$
0.15	16.26	2.96	17.29	1.01	17.15	3.12	18.24	1.07	0.52	$Ba_{0.85}La_{0.15}Ti_{0.92}Al_{0.05}V_{(Ti)0.03}O_3$
0.25	15.79	4.12	17.55	1.60	15.92	4.15	17.69	1.61	0.64	$Ba_{0.79}La_{0.21}Ti_{0.89}Al_{0.08}V_{(Ti)0.03}O_3$
0.30	16.20	5.10	18.27	1.63	15.44	4.86	17.41	1.55	0.83	$Ba_{0.76}La_{0.24}Ti_{0.88}Al_{0.08}V_{(Ti)0.04}O_3$
0.40	15.85	5.27	17.82	1.89	15.25	5.07	17.15	1.82	0.82	$Ba_{0.75}La_{0.25}Ti_{0.87}Al_{0.09}V_{(Ti)0.04}O_3$
0.50	14.84	5.26	16.50	1.44	15.32	5.43	17.03	1.49	0.99	$Ba_{0.74}La_{0.26}Ti_{0.87}Al_{0.08}V_{(Ti)0.05}O_3$

equimolar ratio. The results of WDS analysis are shown in Table 2. In performing the analysis, at least 10 grains in each sample were analyzed. Standard deviations for element concentrations were calculated for particular samples and fall within the range of a maximum of $\pm 2\%$ of the average values given in Table 2. Some higher deviations are observed in samples where the grains analyzed were too small and the influence of microporosity, local topography, and secondary phases on the WDS measurements were high.

The results in Table 2 demonstrate that the concentrations of La^{3+} and Al^{3+} ions in (Ba, La)(Ti, Al)O_3ss depend on the starting $LaAlO_3/BaTiO_3$ ratio and approach saturation above 30 mol% $LaAlO_3$. The ratio of incorporated La^{3+}/Al^{3+} ions in $BaTiO_3$ lattice is approximately 3:1.

Measured concentrations were normalized to 100% (Table 2) and used to calculate the composition of solid solutions. The calculated formulas in Table 2 are based on the assumption that (Ba, La)(Ti, Al)O_3ss contain La on Ba sites and Al on Ti sites in the $BaTiO_3$ lattice. Excess La^{3+} charge on Ba^{2+} sites, which is not compensated by Al^{3+} charge on Ti^{4+} sites, is compensated by V_{Ti}''''. This assumption is supported by WDS analysis which confirmed that [Ba] + [La] > [Ti] + [Al] in all compositions analyzed.

The experimental results make it possible to formulate the mechanism of the $BaTiO_3$–$LaAlO_3$ reaction. La, which is incorporated into $BaTiO_3$ without matching Al, requires a stoichiometric amount of $[Ti_{3/4}(V_{Ti}'''')_{1/4}]$ with corresponding oxygen for the construction of a perovskite lattice. Ti is supplied by $BaTiO_3$. Ba, which is set free, links with Al not incorporated into (Ba, La)(Ti, Al)O_3ss, to form $BaAl_2O_4$. The remaining Ba forms Ba_2TiO_4.

The overall reaction is described by the equation

$$(1-y)BaTiO_3 + (x+y)LaAlO_3 \rightarrow Ba_{1-(x+y)}La_{(x+y)}Ti_{1-((x/4)+y)}Al_y(V_{Ti}'''')_{x/4}O_3 + \frac{x}{2}BaAl_2O_4 + \frac{x}{4}Ba_2TiO_4. \quad [1]$$

Equation [1] is consistent with the results of XRD and WDS analysis.

WDS analysis revealed that $LaAlO_3$ contains some Ba and Ti in (La, Ba)(Al, Ti)O_3ss (not expressed in the equation).

The formation of the parasitic phases $BaAl_2O_4$ and Ba_2TiO_4 in Eq. [1] can be prevented by the addition of excess La_2O_3 and TiO_2 in ratio 2:3 i.e., by the addition of $LaTi_{3/4}O_3$, according to

$$[1-(x+y)]BaTiO_3 + yLaAlO_3 + xLaTi_{3/4}(V_{Ti}'''')_{1/4}O_3 \rightarrow Ba_{1-(x+y)}La_{(x+y)}Ti_{1-((x/4)+y)}Al_y(V_{Ti}'''')_{x/4}O_3. \quad [2]$$

A total of 27 compositions in the ternary $BaTiO_3$–$LaTi_{3/4}O_3$–$LaAlO_3$ system were equilibrated at 1400°C for 40 h. Phases identified by XRD and WDS analysis are listed in Table 3.

The extent of the solid solution region of (Ba, La)(Ti, Al)O_3ss and compatibility relationships with the stable compounds in the $BaTiO_3$–$LaTi_{3/4}O_3$–$LaAlO_3$ system are shown in Fig. 1.

Along the $BaTiO_3$–$LaTi_{3/4}O_3$ tie line, two already reported compounds were confirmed, namely $BaLa_4Ti_4O_{15}$ (5, 13, 14) and $Ba_2La_4Ti_5O_{18}$ (14). $BaLa_4Ti_4O_{15}$ and $Ba_2La_4Ti_5O_{18}$ are compatible with $LaAlO_3$ without appreciable solid solubility.

TABLE 3
XRD Analysis of Samples in the $BaTiO_3$–$LaAlO_3$–$LaTi_{3/4}O_3$ System after Firing at 1400°C

Specimen no.	Composition (mol%) $BaTiO_3$	$LaAlO_3$	$LaTi_{3/4}O_3$	Phases identified[a]
1	90	3	7	BLTAss
2	85	5	10	BLTAss
3	81	5	14	BLTAss
4	80	7	13	BLTAss, BA traces
5	75	5	20	BLTAss
6	75	3	22	BLTAss
7	73	9	18	BLTAss
8	85	10	5	BLTAss, BA
9	82	8	10	BLTAss, BA traces
10	82.5	10	7.5	BLTAss, LBATss traces, BA
11	70	17.5	12.5	BLTAss, LBATss, BA
12	37.5	55	7.5	BLTAss, LBATss
13	70	10	20	BLTAss, LBATss
14	70	5	25	BLTAss, LBATss traces
15	70	2.5	27.5	BLTAss, LBATss
16	50	35	15	BLTAss, LBATss
17	65	5	30	BLTss, LBATss traces
18	57.5	12.5	30	BLTss, LBATss, 225 traces
19	45	30	25	BLTss, LBATss, 225
20	15	77.5	7.5	LBATss, BLTss, 225 traces
21	35	5	60	LBATss, 225, BLTss traces
22	25	10	65	124, 225, LBATss
23	4	80	16	LBATss, 124
24	5	10	85	L_2T_{3ss}, 124, LBATss traces
25	5	3	92	L_2T_{3ss}, 124
26	5	90	5	LBATss, 225
27	3.5	94.5	2	LBATss

[a]BLTAss, $(Ba, La)(Ti, Al)O_3$ solid solution; BLTss, $(Ba, La)TiO_3$ solid solution; LBATss, $(La, Ba)(Al, Ti)O_3$ solid solution; 225, $Ba_2La_4Ti_5O_{18}$; 124, $BaLa_4Ti_4O_{15}$; L_2T_3ss, $LaTi_{3/4}O_3$ solid solution.

In $BaTiO_3$-rich compositions, La replaces up to 30% of Ba ($Ba_{0.7}La_{0.3}Ti_{0.925}O_3$). With an average ratio of Al/La = 0.36 in $(Ba, La)(Ti, Al)O_3$ss, the composition of the solid solution may be expressed as $Ba_{1-n}La_nTi_{1-0.52n}Al_{0.36n}O_3$ with $0 \leq n \leq 0.27$. In the proposed formula, $(Ti + Al) \leq 1$. The difference is due to vacancies at Ti sites, V'''_{Ti}, which compensate the excess La over Al in $(Ba, La)(Ti, Al)O_3$ss.

The region in Fig. 1 limited by $BaTiO_3$, $(Ba, La)(Ti, Al)O_3$ss, and $LaAlO_3$ is multiphase. The phases also include, besides $(Ba, La)(Ti, Al)O_3$ss and $(La, Ba)(Al, Ti)O_3$ss, $BaAl_2O_4$ and Ba_2TiO_4.

Microstructural investigations of the ceramics with selected compositions additionally confirmed the phase relations depicted in Fig. 1. La-rich ceramics with composition within the triangle $BaTiO_3$, $LaAlO_3$, and $(Ba, La)(Ti, Al)O_3$ss (sample 11) are multiphase. At least 3 phases can be detected in the microstructure (Fig. 2); $(La, Ba)(Al, Ti)O_3$ss, $(Ba, La)(Ti, Al)O_3$ss, and $BaAl_2O_4$. The fourth postulated phase (Ba_2TiO_4) is not detectable, probably due to too small amount. This part of the compositional diagram is not ternary. In the $BaTiO_3$-rich part of the same compositional triangle only two phases are detectable in sintered ceramics, i.e., $(Ba, La)(Ti, Al)O_3$ss and $BaAl_2O_4$ (sample 8, Fig. 3).

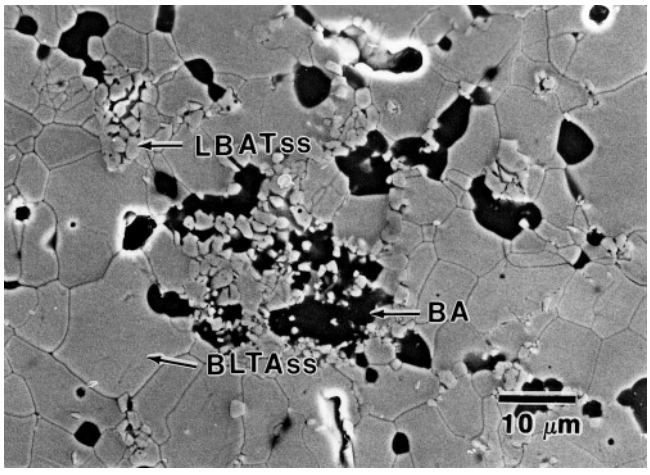

FIG. 2. SEM micrograph of the 0.9 $BaTiO_3$–0.07 $LaTi_{3/4}O_3$–0.03 $LaAlO_3$ composition after firing at 1400°C for 40 h (sample 11 in Fig. 1). BLTAss, $(Ba, La)(Ti, Al)O_3$ solid solution. LBATss, $(La, Ba)(Al, Ti)O_3$ solid solution; BA, $BaAl_2O_4$.

Ceramics with composition within the triangle $BaTiO_3$, $(Ba, La)TiO_3$ss, and $(Ba, La)(Ti, Al)O_3$ss are monophase (sample 1, Fig. 4 and sample 5, Fig. 5).

The difference in grain size of ceramics sintered at 1400°C for 40 h is worth noting. It increases from 5 μm in $BaTiO_3$-rich composition (sample 1) with increasing amount of La and Al to over 15 μm (sample 5).

Multiphase ceramics in the compositional triangle $BaTiO_3$–$LaAlO_3$–$(Ba, La)(Ti, Al)O_3$ss become with increasing amount of $La_{3/4}TiO_3$ 2-phasic (sample 14, Fig. 6) and 3-phasic again (sample 18, Fig. 7). Microstructures are consistent with other observations in this work.

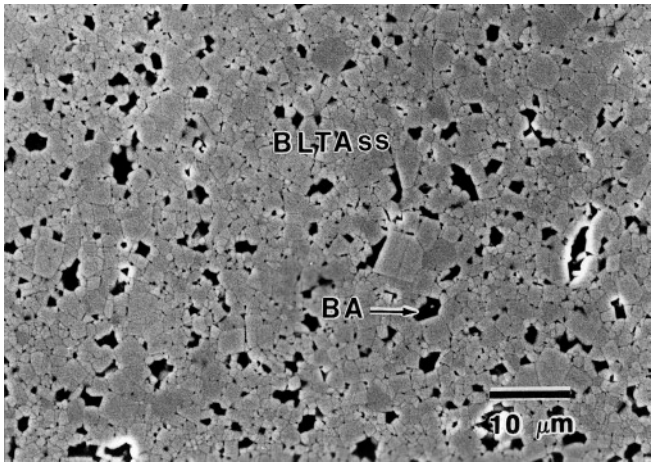

FIG. 3. SEM micrograph of the 0.85 $BaTiO_3$–0.05 $LaTi_{3/4}O_3$–0.1 $LaAlO_3$ composition after firing at 1400°C for 40 h (sample 8 in Fig. 1). BLTAss, $(Ba, La)(Ti, Al)O_3$ solid solution; BA, $BaAl_2O_4$.

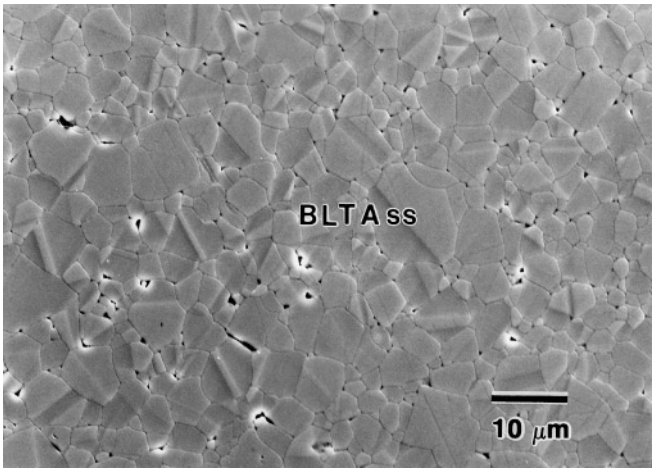

FIG. 4. SEM micrograph of the 0.7 $BaTiO_3$–0.125 $LaTi_{3/4}O_3$–0.175 $LaAlO_3$ composition after firing at 1400°C for 40 h (sample 11 in Fig. 1). BLTAss, (Ba, La)(Ti, Al)O_3 solid solution.

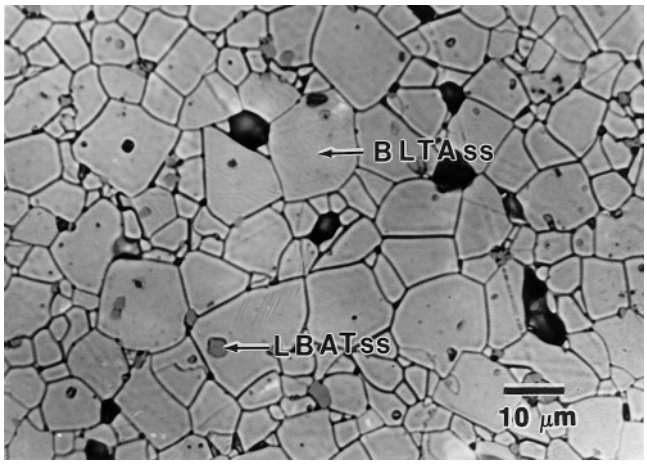

FIG. 6. SEM micrograph of the 0.70 $BaTiO_3$–0.25 $LaTi_{3/4}O_3$–0.05 $LaAlO_3$ composition after firing at 1400°C for 40 h (sample 14 in Fig. 1). BLTAss, (Ba, La)(Ti, Al)O_3 solid solution; LBATss, (La, Ba)(Al, Ti)O_3 solid solution.

3.2. Dielectric Properties

Dielectric properties of the two binary systems $BaTiO_3$–$LaAlO_3$ and $BaTiO_3$–$LaTi_{3/4}O_3$ and a ternary system $BaTiO_3$– $LaAlO_3$–$LaTi_{3/4}O_3$ were measured.

The dielectric properties of ceramics based on the $BaTiO_3$–$LaTi_{3/4}O_3$ system are shown in Fig. 8a. Addition of $LaTi_{3/4}O_3$ to $BaTiO_3$ strongly reduces the Curie temperature of the ceramic. This is in agreement with literature data. It is well known that the rare earth elements incorporated in $BaTiO_3$ structure decrease T_C (20). Four mol% $LaTi_{3/4}O_3$ addition to $BaTiO_3$ shifts T_C from 128°C to room temperature. Further addition of $LaTi_{3/4}O_3$ drastically decreases the room temperature permittivity and dielectric losses (Table 4). A slight improvement in the dielectric properties of such ceramics can be obtained with a small excess of TiO_2, and by applying an oxidizing atmosphere during sintering.

An even stronger shift of T_C was observed in ceramics based on $BaTiO_3$–$LaAlO_3$ systems (Fig. 8b). One mol% $LaAlO_3$ addition to $BaTiO_3$ decreases T_C by $\approx$35°C. T_C was shifted to room temperature with a 3 mol% addition of $LaAlO_3$ to $BaTiO_3$. Again, further addition of $LaAlO_3$ causes a drastic decrease of room temperature permittivity

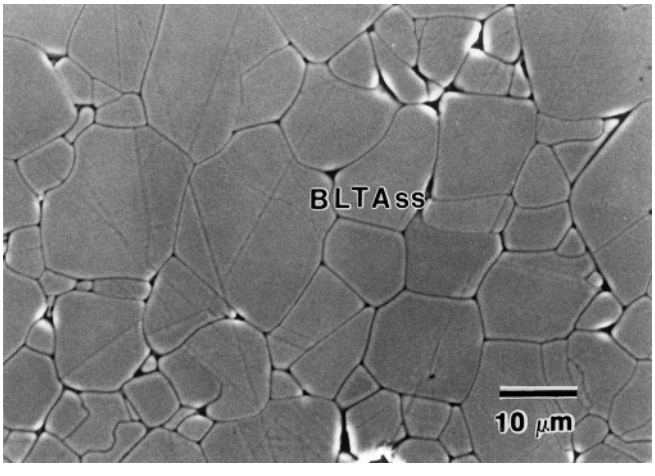

FIG. 5. SEM micrograph of the 0.75 $BaTiO_3$–0.2 $LaTi_{3/4}O_3$–0.05 $LaAlO_3$ composition after firing at 1400°C for 40 h (sample 5 in Fig. 1). BLTAss, (Ba, La)(Ti, Al)O_3 solid solution.

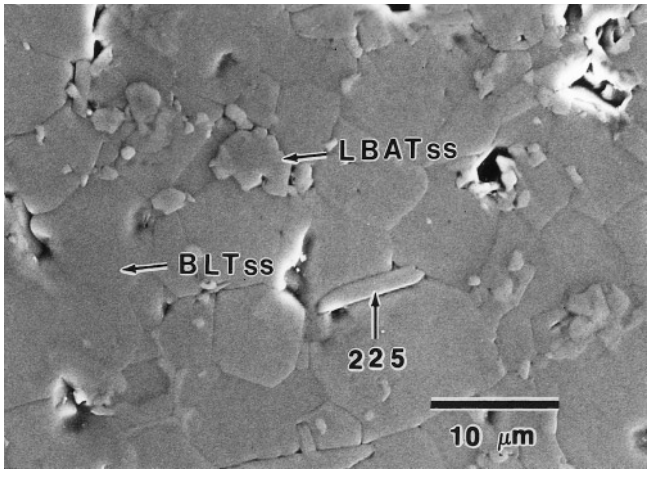

FIG. 7. SEM micrograph of the 0.575 $BaTiO_3$–0.3 $LaTi_{3/4}O_3$–0.125 $LaAlO_3$ composition after firing at 1400°C for 40 h (sample 18 in Fig. 1). BLTss, (Ba, La)TiO_3 solid solution; LBATss, (La, Ba)(Al, Ti)O_3 solid solution; 225, $Ba_2La_4Ti_5O_{18}$.

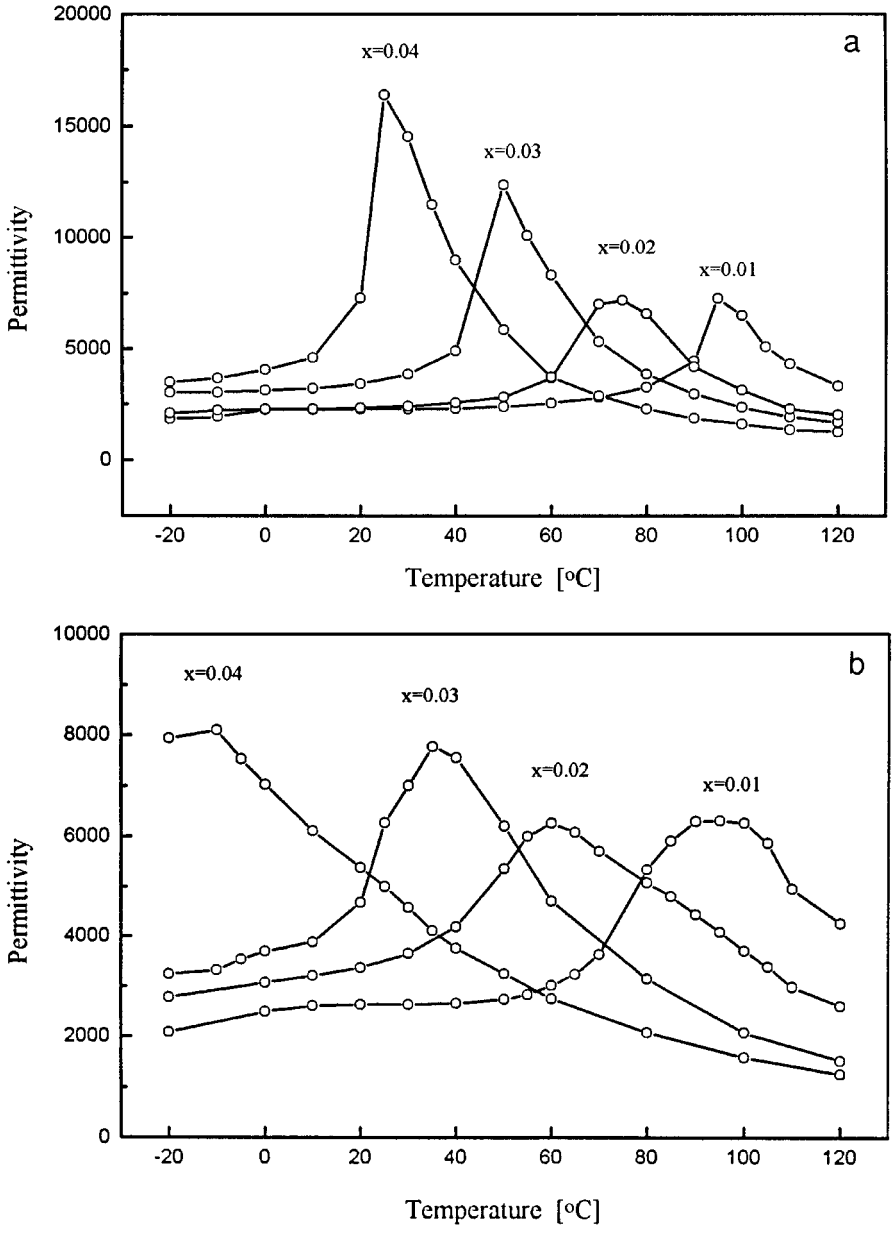

FIG. 8. Temperature dependence of permittivity for (a) $(1-x)BaTiO_3$–$xLaTi_{3/4}O_3$ compositions; (b) $(1-x)BaTiO_3$–$xLaAlO_3$ compositions (measured at 1 MHz).

and dielectric losses (Table 5) which are still higher than in the $BaTiO_3$–$LaTi_{3/4}O_3$ system. Such high dielectric losses in ceramics based on the $BaTiO_3$–$LaAlO_3$ system are probably due to the presence of the secondary phases $BaAl_2O_4$ and Ba_2TiO_4. The more pronounced shift of T_C can be ascribed, according to the proposed reaction scheme, to the incorporation of both La^{3+} and Al^{3+} ions into the $BaTiO_3$ structure during heat treatment (Eq. [1]).

In Table 6, the dielectric properties of monophase ceramics with various compositions based on the $BaTiO_3$–$LaAlO_3$–$LaTi_{3/4}O_3$ system are given. Relatively low permittivities (from 734–129) and low dielectric losses $\tan\delta < 5\times10^{-4}$ characterize such ceramics. The temperature stability of permittivity increases with $LaTi_{3/4}O_3$ as well as with $LaAlO_3$ concentration.

4. CONCLUSIONS

1. $BaTiO_3$ and $LaAlO_3$ react at high temperatures to form (Ba, La)(Ti, Al)O_3ss, $BaAl_2O_4$, and Ba_2TiO_4. In

TABLE 4
Dielectric Constant (*DK*), Loss (tan δ), and Temperature Coefficient of Dielectric Constant (τ_K) of $(1-x)\,BaTiO_3$–$xLaTi_{3/4}O_3$-Based Ceramics (Sintered at 1400°C for 20 h and Measured at 1 MHz)

x in $(1-x)\,BaTiO_3$: $xLaTi_{3/4}O_3$	$DK_{20°C}$	tan $\delta \times 10^4$	τ_K [ppm/K]
0.1	800	10	− 5518
+ 1 wt.% TiO_2	820[a]	7	− 6472
0.15	402	4	− 3838
0.20	254	6	− 2165
0.25	169	4	− 1732
+ 1 wt.% TiO_2	213[a]	7	− 1799
0.30	138	3	− 1346

[a] Sintered in oxygen atmosphere.

TABLE 5
Dielectric Constant (*DK*), Loss (tan δ), and Temperature Coefficient of Dielectric Constant (τ_K) of $(1-x)BaTiO_3$–$xLaAlO_3$-Based Ceramics (Sintered at 1560°C for 20 h and Measured at 1 MHz)

x in $(1-x)\,BaTiO_3$: $x\,LaAlO_3$	$DK_{20°C}$	tan $\delta \times 10^4$	τ_K [ppm/K]
0.1	360	22	− 4540
0.2	143	33	− 1199
0.3	71	29	− 730

(Ba, La)(Ti, Al)O_3ss, $[La^{3+}] > [Al^{3+}]$ and the excess La^{3+} charge on Ba^{2+} sites is compensated by charged Ti vacancies, V'''''_{Ti}. The amounts of La^{3+} and Al^{3+} incorporated into (Ba, La)(Ti, Al)O_3ss depend on the initial $BaTiO_3/LaAlO_3$ ratio. The composition of the solid solution may be expressed as $Ba_{1-n}La_nTi_{1-0.52n}Al_{0.36n}O_3$ with $0 \le n \le 0.27$.

2. The formation of $BaAl_2O_4$ and Ba_2TiO_4 parasitic phases in the $BaTiO_3$–$LaAlO_3$ reaction may be avoided by addition of $LaTi_{3/4}O_3$. In the $BaTiO_3$–$LaAlO_3$–$LaTi_{3/4}O_3$ ternary system an extensive single phase region of (Ba, La)(Ti, Al)O_3ss exists.

3. Incorporation of La and Al into the $BaTiO_3$ lattice strongly shifts the Curie temperature to lower temperatures, by ≈ 35 K/mol% $LaAlO_3$. Ceramics based on (Ba, La)(Ti, Al)O_3ss exhibit low permittivities (from 734–129) and very low dielectric losses tan $\delta < 5 \times 10^{-4}$.

ACKNOWLEDGMENTS

We appreciate the help of Mr. Z. Samardžija for WDS analyses. Financial support from a the U.S.–Slovenian grant (Contract No. 95-351) is gratefully acknowledged.

REFERENCES

1. T. Negas, G. Yeager, S. Bell, and R. Amren, in *Chemistry of Electronic Ceramic Materials* (P. K. Davies and R. S. Roth, Eds.), pp. 21–37, NIST Spec. Publication No. 804, 1991.
2. J. B. MacChesney, P. K. Gallagher, and F. V. DiMarcello, *J. Am. Ceram. Soc.* **46**(5), 197 (1963).
3 J. Daniels and K. H. Härdtl, *Phillips Res. Rep.* **31,** 489 (1976).
4. M. M. Nasrallah, H. U. Anderson, A. K. Agarwal, and B. F. Flandermeyer, *J. Mater. Sci.* **19,** 3159 (1984).

TABLE 6
Dielectric Constant (*DK*), Loss (tan δ), and Temperature Coefficient of Dielectric Constant (τ_K) of $BaTiO_3$–$LaAlO_3$–$LaTi_{3/4}O_3$-Based Ceramics (Sintered at 1400°C for 20 h and Measured at 1 MHz)

	Composition (mol%)					
Sample no.	$BaTiO_3$	$LaAlO_3$	$LaTi_{3/4}O_3$	$DK_{20°C}$	tan $\delta \times 10^4$	τ_K [ppm/K]
1	90	3	7	734	5	− 5527
2	85	5	10	330	< 1	− 3312
				390[a]	1	− 2854
3	81	5	14	193	2	− 2295
				229[a]	1	− 1929
4	80	7	13	180	4	− 1898
5	75	5	20	130	5	− 1484
				144[a]	2	− 1587
6	75	3	22	207	2	− 1530
7	73	9	18	129[a]	3	− 1162
14	70	5	25	121[a]	4	− 1157
15	70	2.5	27.5	66	8	− 1219

[a] Sintered in oxygen atmosphere.

5. G. H. Jonker and E. E. Havinga, *Mater. Res. Bull.* **17,** 345 (1982).
6. G. V. Lewis and C. R. A. Catlow, *J. Phys. Chem. Solids* **47** (1), 89 (1986).
7. A. S. Shaikh and R. W. Vest, *J. Am. Ceram. Soc.* **69** (9), 689 (1986).
8. G. W. Lewis, C. R. A. Catlow, and R. E. W. Casselton, *J. Am. Ceram. Soc.* **68**(10), 555 (1985).
9. S. B. Desu, *Ceramic Transactions* (H. C. Ling, Ed.), Vol. 8. American Ceramic Society, Westerville, OH, 1990.
10. D. Makovec, Z. Samardžija, U. Delalut, and D. Kolar, *J. Am. Ceram. Soc.* **78**(8), 2193 (1995).
11. N. F. Fedorov, O. V. Meljnikova, V. A. Saltikova, and M. V. Chistiakova, *Zh. Neorg. Khim.* **24**(5), 1166 (1979).
12. M. German and L. M. Kovba, *Zh. Neorg. Khim.* **28**(9), 2377 (1983).
13. V. A. Saltikova, O. V. Meljnikova, N. V. Leonova, and N. F. Fedorov, *Zh. Neorg. Khim.* **30**(1), 190 (1985).
14. S. Škapin, D. Kolar, and D. Suvorov, *J. Am. Ceram. Soc.* **76**(9), 2359 (1993).
15. N.-H. Chan, R. K. Sharma, and D. M. Smyth, *J. Am. Cer. Soc.* **65** (3), 167 (1982).
16. S. Geller and V. B. Bala, *Acta Crystallogr.* **9,** 1019 (1956).
17. E. T. Fritsche and L. G. Tensmeyer, *J. Am. Ceram. Soc.* **50**(3), 167 (1967).
18. I. G. Ismailzade, *Izv. Akad. Nauk SSSR Ser. Fiz.* **22**(12), 1483 (1958).
19. G. F. Bastin, H. J. M. Heijligers, and L. J. J. van Loo, *Scanning* **8,** 150 (1986).
20. Von J. Kainz, *Ber. Dt. Keram. Ges.* **35**(3), 69 (1958).